
U-REPA: Aligning Diffusion U-Nets to ViTs

Yuchuan Tian¹, Hanting Chen², Mengyu Zheng³, Yuchen Liang⁴, Chao Xu¹, Yunhe Wang²

¹ State Key Lab of General AI, School of Intelligence Science and Technology, Peking University.

² Huawei Noah's Ark Lab. ³ The University of Sydney. ⁴ School of Mathematical Sciences, Peking University.

tianyc@stu.pku.edu.cn, {chenhan, yunhe.wang}@huawei.com

xuchao@cis.pku.edu.cn

Abstract

Representation Alignment (REPA) that aligns Diffusion Transformer (DiT) hidden-states with ViT visual encoders has proven highly effective in DiT training, demonstrating superior convergence properties, but it has not been validated on the canonical diffusion U-Net architecture that shows faster convergence compared to DiTs. However, adapting REPA to U-Net architectures presents unique challenges: (1) different block functionalities necessitate revised alignment strategies; (2) spatial-dimension inconsistencies emerge from U-Net's spatial downsampling operations; (3) space gaps between U-Net and ViT hinder the effectiveness of tokenwise alignment. To encounter these challenges, we propose **U-REPA**, a representation alignment paradigm that bridges U-Net hidden states and ViT features as follows: Firstly, we propose via observation that due to skip connection, the middle stage of U-Net is the best alignment option. Secondly, we propose upsampling of U-Net features after passing them through MLPs. Thirdly, we observe difficulty when performing tokenwise similarity alignment, and further introduces a manifold loss that regularizes the relative similarity between samples. Experiments indicate that the resulting U-REPA could achieve excellent generation quality and greatly accelerates the convergence speed. With CFG guidance interval, U-REPA could reach $FID < 1.5$ in 200 epochs or 1M iterations on ImageNet 256×256 , and needs only half the total epochs to perform better than REPA. Codes are available at <https://github.com/YuchuanTian/U-REPA>.

1 Introduction

Representation Alignment (REPA) [45], a methodology that aligns features from Diffusion Transformers (DiT) [30] to modern visual encoders, has been demonstrated to significantly accelerate DiT training. This approach holds particular significance given the growing prominence of DiTs, which have gained mainstream adoption in diffusion models and are extensively applied across image generation [4; 11; 23] and video generation domains [48; 22; 19]. However, emerging empirical evidence suggests that U-Net [33] architectures might present a more advantageous alternative to DiTs in certain scenarios [18; 7; 39; 38]: U-Net-based models exhibit substantially faster convergence while achieving generation quality comparable to their transformer-based counterparts. This dichotomy motivates our core research inquiry - can modern Vision Transformer (ViT [10])-based visual encoders be effectively adapted to guide diffusion U-Net training through alignment mechanisms similar to REPA, thereby potentially elevating the convergence speed ceiling of diffusion models?

However, establishing effective alignment between U-Net architectures and ViT-based encoders presents challenges. Unlike Diffusion Transformers (DiTs) that share structural similarities with Vision Transformers, U-Net architectures exhibit fundamentally different operational characteristics. Specifically, both DiT and ViT adopt isotropic architectures composed of uniformly stacked transformer blocks, which inherently facilitates straightforward parameter alignment between the two

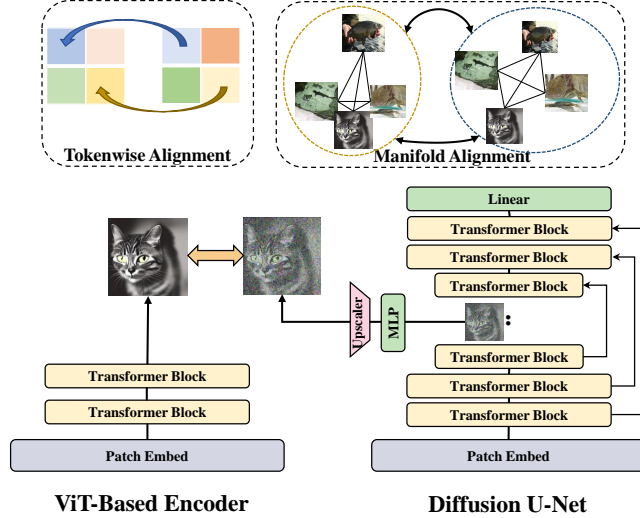


Figure 1: **The proposed U-REPA framework.** We investigated and found that semantic-rich intermediate layers are the best for representation alignment, dimension and space gaps hinders alignment efficacy. To counter these challenges, we scale-up features and propose manifold alignment.

frameworks. In contrast, U-Net’s skip connections create strong interdependencies between shallow and deep network layers by linking them together, resulting in different feature propagation dynamics. This architectural disparity renders conventional representation alignment strategies developed for DiT architectures inapplicable to U-Net frameworks. Furthermore, the progressive downsampling operations in U-Net generate feature maps with spatial dimension mismatches compared to the fixed-scale feature representations in ViT encoders, introducing additional complexity in establishing cross-architectural correspondence. In addition, features from high-stage U-Net and ViT have large space gaps, forming a barrier for cosine similarities as metrics. Forcibly using tokenwise similarity as loss is not necessarily the best option. This induces us to rethink about the optimization objective.

In order to conquer these challenges, we propose **U-REPA**, a framework that aligns U-Net hidden states to features from ViT encoders. Firstly, Our analysis reveals that skip connections fundamentally alter the functional specialization of transformer blocks in U-Net architectures. By establishing direct dependencies between early-stage and late-stage layers, these cross-connections induce a hierarchical redistribution of semantic information, with intermediate blocks exhibiting the highest semantic density. This pattern was empirically verified through controlled ablation studies on DiT augmented with skip connections, where progressive layer-wise evaluations demonstrated peak semantic richness at median network depths.

The intermediate higher-stage layers, which contain semantically dense representations, require precise alignment with the ViT-based visual encoder. However, these critical layers undergo spatial downsampling in the U-Net architecture, necessitating explicit spatial dimension reconciliation between U-Net features and ViT features during representation alignment. Through empirical exploration of various resolution-matching strategies, we identified an optimal solution: performing linear transformation via MLP on U-Net features prior to upsampling operations, which achieves superior alignment performance compared to alternative approaches.

Further analysis revealed a fundamental incompatibility of measuring cosine similarity between the feature spaces of U-Net and ViT encoders. Enforcing strict token-wise similarity constraints proves excessively rigid due to inherent architectural discrepancies. To address this, we introduce a manifold loss that implements soft alignment through relational regularization. This loss operates on the relative geometric relationships between samples rather than imposing direct feature correspondence, thereby accommodating cross-architectural variations. Comprehensive experiments demonstrate that our proposed U-REPA framework effectively bridges the U-Net-ViT alignment gap while preserving the distinct advantages of both architectures.

Our contribution are as follows:

1. We identify U-Net’s representation alignment to be a challenge due to different block functionalities, spatial-dimension inconsistencies, and larger feature space gaps.
2. We evaluate the contribution of downsampling and skips in U-Net and demonstrate U-Net’s potential advantage over DiTs.
3. We propose U-REPA, a framework that evaluates layers, investigates the best scale-up policy, and introduces manifold-space loss in aid of alignment.
4. We conduct experiments and verify the effectiveness of our U-REPA framework in terms of fast convergence. Specifically, U-REPA reaches $FID < 1.5$ in just 200 epochs on ImageNet 256×256 ; and it reaches 1.41 FID, with only half the epochs of REPA under the same training setting.

2 Related Work

The development of diffusion architectures. The conventional diffusion works [17; 35; 36; 9] leverages a U-Net [33] architecture, whose basic block is a concatenation of convolution layers and self-attention. More recent architectural innovations in diffusion models have witnessed a paradigm shift from conventional U-Net frameworks toward transformer-based architectures. The emergence of Diffusion Transformers [1; 30] demonstrates their competitive performance despite abandoning the inductive biases inherent in U-Net designs. U-ViT [1] represents an intermediate architecture that preserves U-Net’s hierarchical structure but replaces convolutional blocks with transformer layers, notably omitting the traditional downsampling operations. Subsequent developments have further streamlined the architecture: DiT [30] adopts a pure transformer backbone with isotropic scaling, while SiT [26] integrates the transformer architecture into the RectifiedFlow framework. Some other works either improve the micro-designs [6; 25], or focuses on architectural efficiency [3; 42; 40].

In contrary to these DiT works, some works still sticks to U-Net architectures and offer valuable rethinking on this conventional architectural preference: in pixel-space image generation, works including SimpleDiffusion [18] and HourglassDiT [7] still sticks to U-Net; in with its variants like U-DiT [39], Playground v3 [24], and DiC [38] extending its success to latent-space diffusion through simple $\text{Conv}3 \times 3$ designs. While these implementations empirically validate U-Net’s accelerated convergence and stable training dynamics compared to transformer-based alternatives, current research predominantly focuses on proposing architectural modifications rather than uncovering the reasons of U-Net’s superior diffusion performance.

Techniques for better DiT performance. Building upon the success of self-supervised learning [16], MDT [13] and MaskDiT [47] pioneer masked image modeling in diffusion frameworks by adaptively masking a good proportion of input patches during training. Other than the masking strategy, a bunch of diffusion works refer to higher-level semantic guidance from off-the-shelf pretrained models that significantly improves generation quality. REPA [45] establishes feature alignment between ViT-based encoder embeddings and diffusion latent spaces through contrastive learning. LightningDiT [44] innovates through an improved VAE distilled from MAE [16] and DINOv2 [28]. Ma et al. [27] introduces CLIP [31] and DINO [2] to verify inference-time scaling of diffusion models. These methods demonstrate that a higher-level semantic-rich feature-map from pretrained vision encoders is helpful to diffusion-based generation.

3 Method

3.1 Preliminaries: REPA for DiT

Representation Alignment (REPA) [45] distills Diffusion Transformers with semantic features from off-the-shelf ViT-based vision encoders (e.g. DINOv2 [28], CLIP [31], MAE [16], et cetera). Given a ViT-based vision encoder f and clean image \mathbf{x}_* , let $\mathbf{y}_* = f(\mathbf{x}_*) \in \mathbb{R}^{N \times D}$ denote its patch embeddings, where N and D represent the number of patches and embedding dimension, respectively. REPA establishes feature alignment between \mathbf{y}_* and the projected diffusion encoder outputs $h_\phi(\mathbf{h}_t)$, where $\mathbf{h}_t = f_\theta(\mathbf{z}_t)$ is the latent representation from the diffusion transformer at timestep t , and h_ϕ is a trainable multilayer perceptron (MLP).

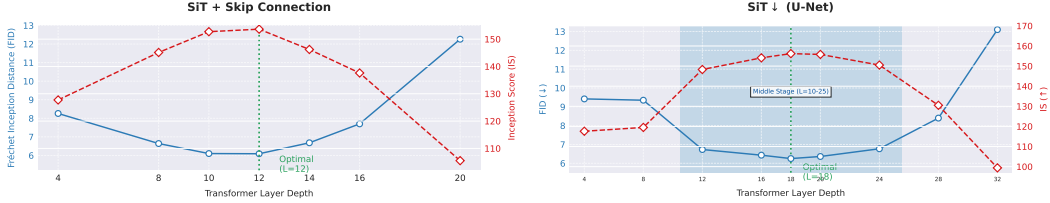


Figure 2: **Investigating alignment with respect to encoder depths on diffusion models with skip connections.** **Left:** SiT with skip connections. Due to the change of block functionalities due to newly established skip dependencies, the most optimal encoder depth is shifted towards the middle of the model. **Right:** SiT \downarrow , the U-Net-based SiT model. Shaded region represents higher U-Net stage. The plot infers that stage transitions (downsampling& upsampling in U-Net) bring large block functionality gaps. Alignment within higher U-Net stage is thus necessary for alignment performance.

The alignment is enforced by maximizing token-wise feature similarities, *i.e.* the similarity of a token from DiT hidden-state with its corresponding counterpart in the ViT encoder feature:

$$\mathcal{L}_{\text{REPA}}(\theta, \phi) := -\mathbb{E}_{\mathbf{x}_*, \epsilon, t} \left[\frac{1}{N} \sum_{n=1}^N \text{sim} \left(\mathbf{y}_*^{[n]}, h_{\phi}(\mathbf{h}_t^{[n]}) \right) \right], \quad (1)$$

where $\text{sim}(\cdot, \cdot)$ denotes a similarity metric (e.g., cosine similarity). Typically, \mathbf{z}_t is adopted as the output from early layers (the original work adopts layer index 8) in DiT for better alignment. This alignment term is combined with the basic flow-based diffusion objective (*i.e.* SiT [26]) through a tunable coefficient $\lambda > 0$, and the final loss for diffusion model training is formulated as follows:

$$\mathcal{L} := \mathcal{L}_{\text{velocity}} + \lambda \mathcal{L}_{\text{REPA}}. \quad (2)$$

3.2 Evaluating the Potential of U-Net

In diffusion models, U-Net and isotropic architectures (e.g., DiT) exhibit distinct design philosophies. While DiT achieves state-of-the-art results through scalability and integration with advanced techniques, U-Net-based methods emphasize faster convergence [39]. To dissect U-Net’s efficacy, we isolate its two core components: skip connections and downsampling.

1. **Skip Connections:** Provide shortcuts between encoder and decoder layers, theoretically aiding gradient flow and feature reuse.
2. **Downsampling:** Reduces spatial resolution (typically by a scale factor of 2 at each stage) to enable hierarchical, multi-scale feature learning. Critically, downsampling is always paired with skip connections to mitigate information loss.

Toy experiments on U-Net components. On top of DiT, we perform toy experiments that reveal the contribution of components mentioned above.

ImageNet 256×256, DiT 400K, cfg=1			
Model	FLOPs (G)	FID↓	IS↑
DiT-XL/2	118.6	19.47	-
DiT-XL/2*	118.6	20.05	66.74
+ Skip Connections	114.1	19.86	67.29
+ Downsampling	108.8	13.78	88.93
DiT\downarrow-XL/2 (+Tricks)	108.8	11.02	100.35

Table 1: **Evaluating the contribution of U-Net components in terms of fast convergence.** Experiments are conducted using hyperparameters from [30] for 400K iterations. Model depth is changed when a modification is made such that the overall FLOPs is kept almost the same with DiT.

This suggests that U-Net’s fast-convergence advantages primarily stem from multi-scale hierarchical modeling via downsampling, not skip connections. Downsampling compresses features into compact, semantically rich representations, accelerating learning while maintaining information flow through skip-augmented decoder layers. However, skip connection is not useless as it compensates for the information loss due to downsampling.

Building on this insight, we propose DiT↓ (and SiT↓ for the flow-based version, following the naming convention of [26]) by adding tricks of RoPE [37] and SwiGLU following previous work [6; 39]

3.3 Aligning U-Net to ViT Encoders

Since U-Net has good potentials to achieve excellent generation, we are motivated to investigate whether REPA could also work on U-Net. We are first focused on the block functionality pattern and investigates the most optimal position for alignment; then we are interested in feature size alignment problems; lastly, we are dedicated to merging space gaps between features from U-Net and ViT, respectively.

Position for alignment. Regarding the concern that block functionalities differ between U-Net and DiT, the comparison of prior studies [12; 5] demonstrates divergent hierarchical specialization: U-Net architectures typically employ mid-network layers for high-level semantic synthesis while reserving shallow layers for low-level image refinement, whereas DiTs exhibit a totally different pattern - early layers primarily govern semantic-rich outline formation with deeper layers handling detailed image refinement.

These previous findings find empirical support in REPA’s experimental findings, where representation alignment proves most effective when applied to initial transformer blocks. This phenomenon stems from DiT’s early layers encoding semantic-rich representations that align well with the semantically dense outputs of ViT-based visual encoders, enabling meaningful guidance. Unlike the straightforward DiT architecture, the inherent skip connections in U-Net architectures induce fundamentally distinct block functionality compared to Diffusion Transformers. While all blocks in ViT or DiT maintain homogeneous computational roles, following a continuous flow of transition from input to output, U-Net’s cross-layer shortcuts establish direct dependencies between shallow and deep layers, fundamentally altering feature-map evolution patterns. As shown in Fig. 2 (R), DiTs with skips indicates median layer is the best for representation alignment. The same pattern goes for U-Net (Fig. 2 (L)) despite the downsampling stage.

Feature size alignment. The implementation of alignment between Diffusion U-Net’s median stage and ViT encounters a critical spatial resolution dilemma stemming from architectural disparities. While our analysis identifies mid-network U-Net features as optimal semantic carriers, their spatial dimensions drastically differ from ViT’s full-resolution token sequence. This dimensional mismatch obstructs REPA’s token-wise similarity computation, which requires strict cardinality matching between compared features.

In order to align two feature-maps (*i.e.* from U-Net and ViT encoder, respectively), from the macro level we advocate for upscaling the smaller-sized U-Net features rather than downscaling the larger visual encoder features. This design principle stems from the critical observation that compressing ViT’s high-resolution features to match U-Net’s reduced dimensions inevitably discards fine-grained visual information, thereby degrading alignment effectiveness. Preserving ViT’s native resolution while expanding U-Net’s bottleneck features proves essential for maintaining semantic fidelity.

At the implementation level, we empirically evaluated various upscaling strategies for U-Net features:

1. **Upscale first and then MLP:** feature upsampling is performed before passing the feature into the MLP.
2. **Upscale within MLP:** the MLP also acts as a feature upsampler that receives a low-resolution input and outputs a high-resolution one via linear mapping and pixel un-shuffling.
3. **MLP first and then upscale:** the feature from higher-stage U-Net is first passed through MLP and then upsampled.

Among the three options, we found “MLP first and then upscale” is the best both in terms of performance and efficiency (minimum FLOPs cost), which will be discussed in the Ablation Study in Sec. 4.

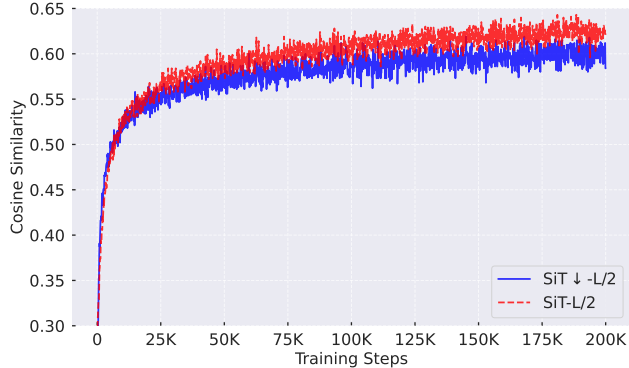


Figure 3: **The convergence of average tokenwise similarities.** While SiT-L/2 could achieve better tokenwise similarities, SiT \downarrow converges at a lower similarity value, indicating difficulties of feature alignment.

Manifold space alignment. Though we select the most suitable U-Net feature for alignment and keep dimensions between U-Net and ViT features aligned, challenges remain in feature space compatibility. First, compared to the structural congruence between DiT and ViT encoders, the architectural discrepancy of U-Net (with its skip connections and hierarchical downsampling) creates a more pronounced feature distribution gap between U-Net hidden states and visual encoder outputs. Second, the dimensional transformation required for alignment inevitably modifies U-Net’s native feature space characteristics.

Some recent works on Diffusion U-Net [41; 34] reveals that higher-stage U-Net features are low-frequency subspaces that discards higher frequency components, including noises. Gaps are inevitable when evaluating the cosine similarities of detail-rich, high-frequency-rich vectors and flat, low-frequency-dominated vectors. In this sense, strict token-level alignment constraints like the original REPA loss prove suboptimal under these conditions, as they assume implicit feature space homogeneity between aligned modalities.

As is shown in Fig. 3, we conducted continuous measurements of token-wise cosine similarity against ViT features during training. The two models that we compare are SiT-L/2 of isotropic, standard transformer architecture and SiT \downarrow -L/2 of U-Net architecture. Our experiments revealed a characteristic learning trajectory: while U-Net achieves slightly faster similarity improvement in early training phases - thanks to skip connection that helps convergence - its progress stagnates beyond this point, ultimately plateauing at 0.60 - notably inferior to DiT’s sustained growth reaching around 0.63 similarity. The similarity gap between SiT and SiT \downarrow . This phenomenon suggests that naively aligning U-Net with ViT encoders through angular similarity metrics alone encounters inherent limitations due to architectural incompatibilities.

Rather than strict token-wise regularization, we resort to looser objectives that does not require rigid angular alignment. Inspired by manifold knowledge distillation [14], we hold that aligning similarities between samples from the same feature space could be a promising solution. Hence, we define Manifold Loss \mathcal{L}_{ML} as

$$\mathcal{L}_{ML}(\theta, \phi) := -\mathbb{E}_{\mathbf{x}_*, \epsilon, t, i, j} [d(\mathbf{y}_*, h_\phi(\mathbf{h}_t))], \quad (3)$$

where

$$d := \|\text{sim}(\mathbf{y}_*^{[i]}, \mathbf{y}_*^{[j]}) - \text{sim}(h_\phi(\mathbf{h}_t^{[i]}), h_\phi(\mathbf{h}_t^{[j]}))\|_F^2. \quad (4)$$

In the formula, cosine similarity is adopted as the similarity metric, and F represents Frobenius Norm of matrices. By introducing affine hyperparameter w , the overall optimization target is then formulated as

$$\mathcal{L} := \mathcal{L}_{\text{velocity}} + \lambda (\mathcal{L}_{\text{REPA}} + w\mathcal{L}_{ML}). \quad (5)$$

3.4 Other Improvements

We also propose and evaluate some other improvements as follows. Due to page limits, the corresponding ablations are enclosed in the Appendix.

Time-aware MLP. Some works on in the diffusion task [29; 46] reveals that a channel dimension is particularly sensitive and useful to a certain subset of time during sampling. As the time-variant feature is to be aligned to time-invariant vision encoder features, we hold that alignment could perform better when the MLP is time-aware and extract time-invariant information out of diffusion features for alignment.

Inspired by the conditioning of canonical Diffusion U-Net [17; 36; 9] and DiT [30], we add a module to predict a pair of channel-wise shift& scale vector $(\gamma(t), \beta(t))$. The module is in parallel to MLP and follows the design of DiT’s AdaLN, which is a concatenation of a SiLU and a Linear layer. The shift& scale vectors are imposed on the output MLP as follows:

$$h_{\phi}^t(\mathbf{h}_t^{[n]}) = \gamma(t) \odot h_{\phi}(\mathbf{h}_t^{[n]}) + \beta(t)$$

Weight schedule of loss. As is prompted in REPA [45], designing weight schedule is a future direction. We try various weight schedules (*i.e.* make λ in Eq. 2 a function $\lambda(t)$ with respect to time) but found that these schedules bring very limited improvements on the proposed U-REPA. Hence, we stick to the original constant weight strategy of REPA.

4 Experiments

4.1 Experiment Setup

Experiment settings. Our implementation completely adheres to the training protocol established in REPA [45]. Following the architectural configuration of latent diffusion models [32], we employ the identical VAE variant (*sd-vae-ft-ema*) and adopt the AdamW optimizer. To ensure fair comparison, we maintain identical hyperparameter settings across all experiments: a global batch size of 256, fixed learning rate of $1e - 4$, and disabled weight decay (set to 0). (β_1, β_2) is set as (0.9, 0.999). All experiments are conducted on the ImageNet 2012 benchmark [8] under a controlled environment with a fixed random seed (global seed=0).

For main experiments (Tab. 4), we apply guidance interval [21] $[0, 0.7]$ and SDE sampling according to the convention of REPA [45] for fair comparison. We select smaller *cfg* of 1.65, because we found it is better for our architecture, different from SiT. For all ablation experiments, we train models for 100K iterations, which is sufficient to show the trend of model performance; sampling is conducted with the default setting of the official REPA codebase, *i.e.* $cfg = 1.8$ in ODE and guidance interval $[0, 0.7]$.

Model settings. By aligning channel dimensions and FLOPs with standard Diffusion Transformers (DiTs or SiTs), our U-REPA-compatible variants maintain architectural parity while introducing critical adaptations for U-Net principles. The base model (SiT \downarrow -B) employs a stage arrangement of [5,5,5], achieving 199.7G FLOPs. Scaling to larger models, we have the L variant (686.6M) and XL variant (954.4M params) that increases channel width (1024 vs. 1152 in base) through increased stage-wise block allocation ([9,14,9] vs. [10,16,10]). Notably, when FLOPs are aligned, SiT \downarrow models usually have more parameters than SiTs due to increased depth.

Model	Params (M)	FLOPs (G)	Patch Size	Channel	# Heads	Blocks in Stages
SiT\downarrow-B	199.7	24.1	2	768	12	[5,5,5]
SiT\downarrow-L	686.6	79.3	2	1024	16	[9,14,9]
SiT\downarrow-XL	954.4	109.3	2	1152	16	[10,16,10]

Table 2: **Configurations of SiT \downarrow architecture at different model sizes.** The proposed SiT \downarrow in U-Net architectures are aligned to DiTs in terms of FLOPs and channel dimension.

ImageNet 256×256, w/o cfg			
Model	FLOPs (G)	Iter.	FID↓
SiT-B/2+REPA	23.0	400K	24.4
SiT↓-B/2+U-REPA	24.1	400K	15.3
SiT-L/2+REPA	80.8	700K	8.4
SiT↓-L/2+U-REPA	79.3	400K	5.8
SiT-XL/2+REPA	118.6	4M	5.9
SiT↓-XL/2+U-REPA	108.8	400K	5.4

Table 3: **Comparing U-REPA against REPA across various model sizes without classifier-free guidance.** U-Nets equipped with U-REPA show excellent capabilities. Notably, U-REPA achieves 10× faster convergence compared with REPA in terms of performance w/o CFG.

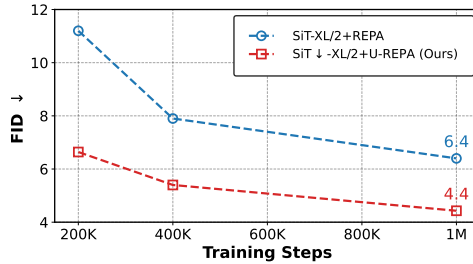


Figure 4: **Comparing SiT↓+U-REPA against SiT+REPA in terms of convergence speed.** SiT↓-XL/2 converges much faster than SiT-XL/2 with the help of U-REPA.

4.2 The Advantage of U-REPA

Comparing SiT↓ with SiT at different scales. We evaluate our U-REPA alignment method on ImageNet 256 under a generation setting with $cfg = 1$ (REPA framework without classifier-free guidance). As shown in Table 3, our approach consistently improves generation quality while significantly reducing computational costs across model scales. For the base-size SiT-B/2 variant, integrating U-REPA achieves a 39.3% improvement in FID (from 24.4 to 15.3) with comparable FLOPs (24.1G vs. 23.0G) and identical training iterations (400K), demonstrating that feature alignment enhances parameter efficiency without additional training overhead. The acceleration effect becomes more pronounced in larger models: for SiT-L/2, U-REPA reduces required iterations by 42.9% (700K→400K) while simultaneously lowering FLOPs (79.3G vs. 80.8G) and achieving a 30.9% FID improvement (8.4→5.8). Most notably, the XL-scale variant with U-REPA (*cf.* Fig. 4 for FIDs vs. Training iters) attains state-of-the-art FID (5.4) using **90%** fewer iterations (400K vs. 4M) and fewer FLOPs (108.8G vs. 118.6G) compared to the baseline, proving our method’s fast convergence.

We also demonstrate the advantage of the proposed U-REPA framework when measuring by parameters (rather than computation FLOPs), as shown in Fig. 5. Though U-Net brings extra parameters when FLOPs are aligned with DiTs, the advantage of SiT↓+U-REPA is obvious as depicted in the Parameter versus FID plot.

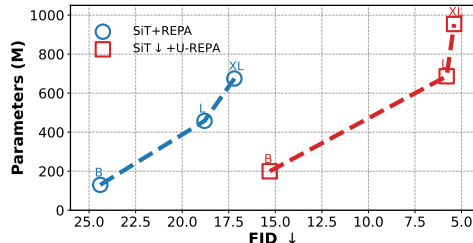


Figure 5: **Comparing SiT↓+U-REPA against SiT+REPA in terms of parameter scalability.** While the U-Net architecture makes the diffusion model parameter-rich compared with same-FLOPs Diffusion Transformers, SiT↓ models still outcompetes SiTs by large margins in terms of parameters.

ImageNet 256×256, w/ cfg		
Model	Epochs	FID↓
<i>Pixel diffusion</i>		
ADM-U [9]	400	3.94
VDM++ [20]	560	2.40
Simple diffusion [18]	800	2.77
<i>Latent Diffusion Transformer</i>		
U-ViT-H/2 [1]	240	2.29
DiffiT [15]	-	1.73
DiT-XL/2 [30]	1400	2.27
SiT-XL/2 [26]	1400	2.06
<i>Masked Diffusion Transformer</i>		
MaskDiT [47]	1600	2.28
MDTv2-XL/2 [13]	1080	1.58
<i>Representation Alignment</i>		
SiT-XL/2 + REPA [45]	800	1.42
SiT↓-XL/2 + U-REPA (Ours)	200	1.48
SiT↓-XL/2 + U-REPA (Ours)	400	1.41

Table 4: **Comparing U-REPA against State-of-the-Art baselines with classifier-free guidance.** U-REPA could reach $FID < 1.5$ within merely 200 epochs; The proposed method converge $2\times$ faster while achieving lower FID.

Convergence performance. We also compare our method with previous State-of-the-Arts, as shown in Tab. 4. Our proposed SiT↓+U-REPA achieves a competitive FID of 1.48 with only 200 training epochs, significantly outperforming existing methods in training efficiency. Notably, while state-of-the-art masked diffusion transformers like MDTv2-XL/2 require 1,080 epochs to reach 1.58 FID, our method attains better performance (1.48) with 80% fewer iterations. Even compared to the SOTA SiT-XL/2 + REPA baseline (800 epochs for 1.42 FID), our approach uses only 1/2 of the training epochs (400) while achieving better generation quality (1.41 FID). The results demonstrate that the proposed U-REPA establishes a new efficiency frontier for diffusion models.

ImageNet 256×256, w/ cfg				
Model	Layer	Feat. Dim.	FID↓	IS↑
SiT↓-XL/2	4	16	9.42	117.6
SiT↓-XL/2	8	16	9.35	119.5
SiT↓-XL/2	12	8	6.73	148.3
SiT↓-XL/2	16	8	6.43	154.1
SiT↓-XL/2	18	8	6.25	156.2
SiT↓-XL/2	20	8	6.36	155.8
SiT↓-XL/2	24	8	6.77	150.5
SiT↓-XL/2	28	16	8.40	130.5
SiT↓-XL/2	32	16	13.10	99.4

Table 5: **Ablations on encoder depths for alignment in SiT↓.** Feat. Dim. stands for the spatial height& width at the certain layer. Aligning at the centering layer (higher stage in U-Net) gets the best result.

4.3 Ablation Studies

Encoder depths. The ablation study on encoder layer depths for feature alignment (Tab. 5) coincides with the pattern of DiT with skip connections, as we analyzed in Sec. 4: despite progressive down-sampling operations that reduce spatial resolution, the centermost layers exhibit optimal alignment efficacy. For the SiT↓-XL/2 model, aligning features at layer 18 (midway through the 36-layer architecture) achieves peak performance with 6.25 FID and 156.2 IS, outperforming both shallower and deeper alignment points. This phenomenon persists even as the spatial dimension (Feat. Dim.)

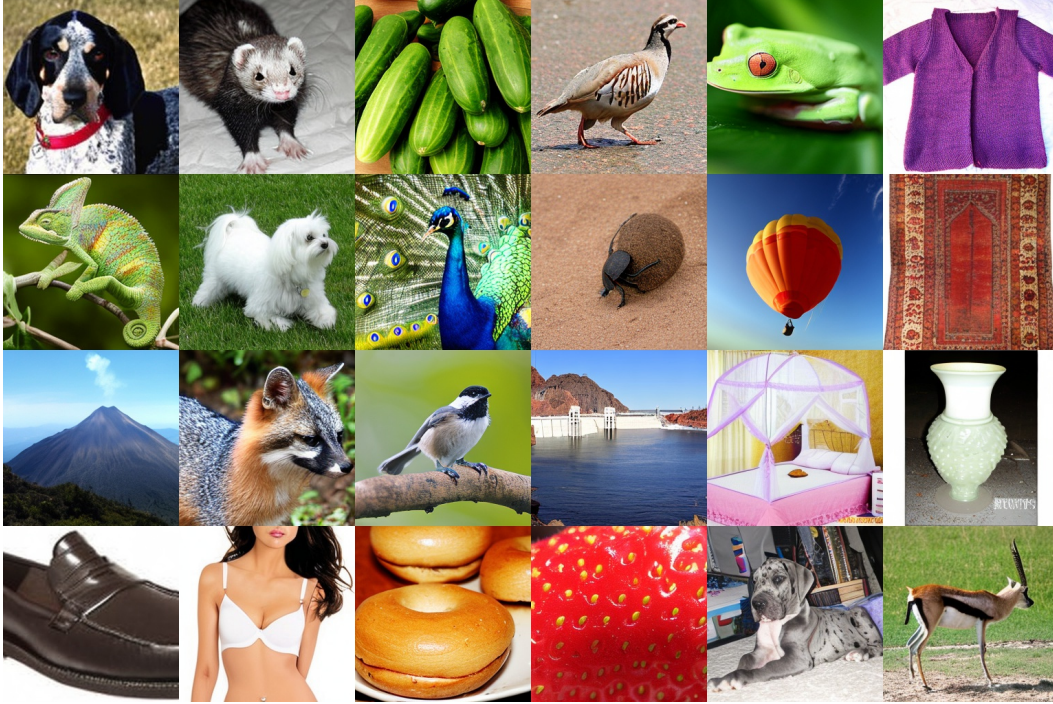


Figure 6: **Samples generated by SiT \downarrow +U-REPA at 1M iterations.** The samples are generated following the setting of REPA, at $cfg = 4$. Best viewed on screen.

halves from 16×16 to 8×8 in the intermediate stage, indicating that semantic richness—not spatial resolution—dominates alignment quality. Performance degradation occurs when alignment takes place at shallower or deeper stages, even though the feature size is kept the same with DINO in these stages.

ImageNet 256×256 , w/ cfg		
Alignment Choices	FID \downarrow	IS \uparrow
U-Net DINOv2 \downarrow_2	5.99	158.8
U-Net \uparrow_2 DINOv2	5.72	161.6

Table 6: **Alignment dimension choices.** Upsampling higher-stage U-Net features in alignment with ViT performs better due to less information loss.

Alignment dimension choices. The comparative results in Table 6 reveal that upsampling U-Net’s higher-stage features (\uparrow_2) to match DINOv2’s native resolution achieves superior performance (5.72 FID, 161.6 IS), outperforming the alignment alternative in generation quality. This demonstrates that preserving ViT encoder’s original feature granularity during alignment is beneficial for alignment.

ImageNet 256×256 , w/ cfg		
Alignment	FID \downarrow	IS \uparrow
Upscale before MLP	5.84	158.5
Upscale in MLP	6.36	153.4
Upscale after MLP	5.72	161.6

Table 7: **Feature-map upscale choices.** Among the three options, Upscaling after passing through MLP performs best; and it has lower cost as the small-sized feature map is passed through MLP.

Feature-map upscale choices. Among the three upscaling options mentioned in Sec. 4, we figure out that upscaling U-Net hidden states after getting passed through MLP is the best option, achieving 5.72 FID and 161.6 IS. This option is also the most optimal one in terms of computation cost analysis:

unlike the other two options, the downsampled size of the feature is kept throughout the whole MLP mapping process, making computation much cheaper. Overall, "Upscale after MLP" is adopted.

ImageNet 256×256, w/ cfg			
Model	w	FID↓	IS↑
SiT↓-XL/2+U-REPA	0	6.25	156.2
SiT↓-XL/2+U-REPA	2	5.81	160.8
SiT↓-XL/2+U-REPA	3	5.72	161.6
SiT↓-XL/2+U-REPA	4	5.79	160.6

Table 8: **Adjusting weight w in Eq. 5.** Manifold loss boosts U-Net’s alignment performance. The most optimal result is taken at $w = 3$.

Manifold loss weight w . The ablation study on alignment weight w in Eq. 5 demonstrates a clear performance peak at $w = 3$ achieving the lowest FID (5.72) and highest IS (161.6) among tested configurations. This optimal weighting balances the alignment objective with the primary REPA loss and diffusion loss. Insufficient regularization ($w < 3$) limits feature space coordination (FID: 6.25→5.81), while overemphasis ($w = 4$) causes FID to regress to 5.79. Overall, we adopt $w = 3$ in our training.

5 Conclusion

In this paper, we propose U-REPA, an adapted version of REPA on Diffusion U-Net that achieves State-of-the-Art convergence speed. We first reveal the potential of U-Net and raise a series of challenges in terms of U-Net hidden state alignment. Our systematic investigation establishes that the U-REPA framework effectively bridges the architectural gap between U-Net-based diffusion models and ViT-based visual encoders. By introducing feature alignment at U-Net’s intermediate layers, resolving spatial incompatibility through post-MLP upsampling, and enforcing manifold-aware similarity regularizations, U-REPA achieves acceleration in training convergence while achieving an FID score of 1.41 on ImageNet-256×256. This work not only demonstrates the viability of integrating ViT-aligned representations into classical U-Net architectures but also reveals the critical role of hierarchical U-Net architecture to fast training convergence. Both extensive experiments and visual demonstrations validate the efficacy of the proposed U-REPA.

Future work. The U-Net architecture is a simple one with only one intermediate stage. We do not further refine the architecture as we want to show U-Net architectures as simple as SiT↓ could also achieve rapid convergence. Further improvements on the U-Net architecture includes efficient attention [42; 39], non-integer down& up scaling factors [43], and more use of convolutions [36; 38]. Besides, whether U-REPA could be applied to downstream diffusion tasks that rely heavily on U-Nets (e.g. Low-Level Vision) remains to be investigated.

References

- [1] Fan Bao, Shen Nie, Kaiwen Xue, Yue Cao, Chongxuan Li, Hang Su, and Jun Zhu. All are worth words: A vit backbone for diffusion models. In *IEEE/CVF Conference on Computer Vision and Pattern Recognition, CVPR 2023, Vancouver, BC, Canada, June 17-24, 2023*, pages 22669–22679. IEEE, 2023.
- [2] Mathilde Caron, Hugo Touvron, Ishan Misra, Hervé Jégou, Julien Mairal, Piotr Bojanowski, and Armand Joulin. Emerging properties in self-supervised vision transformers. In *2021 IEEE/CVF International Conference on Computer Vision, ICCV 2021, Montreal, QC, Canada, October 10-17, 2021*, pages 9630–9640. IEEE, 2021.
- [3] Junsong Chen, Chongjian Ge, Enze Xie, Yue Wu, Lewei Yao, Xiaozhe Ren, Zhongdao Wang, Ping Luo, Huchuan Lu, and Zhenguo Li. Pixart- Σ : Weak-to-strong training of diffusion transformer for 4k text-to-image generation. *CoRR*, abs/2403.04692, 2024.
- [4] Junsong Chen, Jincheng Yu, Chongjian Ge, Lewei Yao, Enze Xie, Yue Wu, Zhongdao Wang, James Kwok, Ping Luo, Huchuan Lu, and Zhenguo Li. Pixart- α : Fast training of diffusion transformer for photorealistic text-to-image synthesis, 2023.

- [5] Pengtao Chen, Mingzhu Shen, Peng Ye, Jianjian Cao, Chongjun Tu, Christos-Savvas Bouganis, Yiren Zhao, and Tao Chen. δ -dit: A training-free acceleration method tailored for diffusion transformers, 2024.
- [6] Xiangxiang Chu, Jianlin Su, Bo Zhang, and Chunhua Shen. Visionllama: A unified llama interface for vision tasks. *CoRR*, abs/2403.00522, 2024.
- [7] Katherine Crowson, Stefan Andreas Baumann, Alex Birch, Tanishq Mathew Abraham, Daniel Z. Kaplan, and Enrico Shippole. Scalable high-resolution pixel-space image synthesis with hourglass diffusion transformers. *CoRR*, abs/2401.11605, 2024.
- [8] Jia Deng, Wei Dong, Richard Socher, Li-Jia Li, Kai Li, and Li Fei-Fei. Imagenet: A large-scale hierarchical image database. In *2009 IEEE Computer Society Conference on Computer Vision and Pattern Recognition (CVPR 2009)*, 20-25 June 2009, Miami, Florida, USA, pages 248–255. IEEE Computer Society, 2009.
- [9] Prafulla Dhariwal and Alexander Quinn Nichol. Diffusion models beat gans on image synthesis. In Marc’Aurelio Ranzato, Alina Beygelzimer, Yann N. Dauphin, Percy Liang, and Jennifer Wortman Vaughan, editors, *Advances in Neural Information Processing Systems 34: Annual Conference on Neural Information Processing Systems 2021, NeurIPS 2021, December 6-14, 2021, virtual*, pages 8780–8794, 2021.
- [10] Alexey Dosovitskiy, Lucas Beyer, Alexander Kolesnikov, Dirk Weissenborn, Xiaohua Zhai, Thomas Unterthiner, Mostafa Dehghani, Matthias Minderer, Georg Heigold, Sylvain Gelly, Jakob Uszkoreit, and Neil Houlsby. An image is worth 16x16 words: Transformers for image recognition at scale. *CoRR*, abs/2010.11929, 2020.
- [11] Patrick Esser, Sumith Kulal, Andreas Blattmann, Rahim Entezari, Jonas Müller, Harry Saini, Yam Levi, Dominik Lorenz, Axel Sauer, Frederic Boesel, Dustin Podell, Tim Dockhorn, Zion English, and Robin Rombach. Scaling rectified flow transformers for high-resolution image synthesis. In *Forty-first International Conference on Machine Learning*, 2024.
- [12] Gongfan Fang, Xinyin Ma, and Xinchao Wang. Structural pruning for diffusion models. In Alice Oh, Tristan Naumann, Amir Globerson, Kate Saenko, Moritz Hardt, and Sergey Levine, editors, *Advances in Neural Information Processing Systems 36: Annual Conference on Neural Information Processing Systems 2023, NeurIPS 2023, New Orleans, LA, USA, December 10 - 16, 2023*, 2023.
- [13] Shanghua Gao, Pan Zhou, Ming-Ming Cheng, and Shuicheng Yan. Mdtv2: Masked diffusion transformer is a strong image synthesizer, 2024.
- [14] Zhiwei Hao, Jianyuan Guo, Ding Jia, Kai Han, Yehui Tang, Chao Zhang, Han Hu, and Yunhe Wang. Learning efficient vision transformers via fine-grained manifold distillation. In Sanmi Koyejo, S. Mohamed, A. Agarwal, Danielle Belgrave, K. Cho, and A. Oh, editors, *Advances in Neural Information Processing Systems 35: Annual Conference on Neural Information Processing Systems 2022, NeurIPS 2022, New Orleans, LA, USA, November 28 - December 9, 2022*, 2022.
- [15] Ali Hatamizadeh, Jiaming Song, Guilin Liu, Jan Kautz, and Arash Vahdat. Diffit: Diffusion vision transformers for image generation. *CoRR*, abs/2312.02139, 2023.
- [16] Kaiming He, Xinlei Chen, Saining Xie, Yanghao Li, Piotr Dollár, and Ross B. Girshick. Masked autoencoders are scalable vision learners. In *IEEE/CVF Conference on Computer Vision and Pattern Recognition, CVPR 2022, New Orleans, LA, USA, June 18-24, 2022*, pages 15979–15988. IEEE, 2022.
- [17] Jonathan Ho, Ajay Jain, and Pieter Abbeel. Denoising diffusion probabilistic models. *CoRR*, abs/2006.11239, 2020.
- [18] Emiel Hoogeboom, Jonathan Heek, and Tim Salimans. simple diffusion: End-to-end diffusion for high resolution images. In Andreas Krause, Emma Brunskill, Kyunghyun Cho, Barbara Engelhardt, Sivan Sabato, and Jonathan Scarlett, editors, *International Conference on Machine Learning, ICML 2023, 23-29 July 2023, Honolulu, Hawaii, USA*, volume 202 of *Proceedings of Machine Learning Research*, pages 13213–13232. PMLR, 2023.
- [19] Yang Jin, Zhicheng Sun, Ningyuan Li, Kun Xu, Hao Jiang, Nan Zhuang, Quzhe Huang, Yang Song, Yadong Mu, and Zhouchen Lin. Pyramidal flow matching for efficient video generative modeling. *CoRR*, abs/2410.05954, 2024.
- [20] Diederik P. Kingma and Ruiqi Gao. Understanding diffusion objectives as the ELBO with simple data augmentation. In Alice Oh, Tristan Naumann, Amir Globerson, Kate Saenko, Moritz Hardt, and Sergey Levine, editors, *Advances in Neural Information Processing Systems 36: Annual Conference on Neural Information Processing Systems 2023, NeurIPS 2023, New Orleans, LA, USA, December 10 - 16, 2023*, 2023.

- [21] Tuomas Kynkäänniemi, Miika Aittala, Tero Karras, Samuli Laine, Timo Aila, and Jaakko Lehtinen. Applying guidance in a limited interval improves sample and distribution quality in diffusion models. In Amir Globersons, Lester Mackey, Danielle Belgrave, Angela Fan, Ulrich Paquet, Jakub M. Tomczak, and Cheng Zhang, editors, *Advances in Neural Information Processing Systems 38: Annual Conference on Neural Information Processing Systems 2024, NeurIPS 2024, Vancouver, BC, Canada, December 10 - 15, 2024*, 2024.
- [22] PKU-Yuan Lab and Tuzhan AI etc. Open-sora-plan, April 2024.
- [23] Black Forest Labs. Flux, August 2024.
- [24] Bingchen Liu, Ehsan Akhgari, Alexander Visheratin, Aleks Kamko, Linmiao Xu, Shivam Shrirao, Chase Lambert, Joao Souza, Suhail Doshi, and Daiqing Li. Playground v3: Improving text-to-image alignment with deep-fusion large language models, 2024.
- [25] Zeyu Lu, Zidong Wang, Di Huang, Chengyue Wu, Xihui Liu, Wanli Ouyang, and Lei Bai. Fit: Flexible vision transformer for diffusion model. *CoRR*, abs/2402.12376, 2024.
- [26] Nanye Ma, Mark Goldstein, Michael S. Albergo, Nicholas M. Boffi, Eric Vanden-Eijnden, and Saining Xie. Sit: Exploring flow and diffusion-based generative models with scalable interpolant transformers. *CoRR*, abs/2401.08740, 2024.
- [27] Nanye Ma, Shangyuan Tong, Haolin Jia, Hexiang Hu, Yu-Chuan Su, Mingda Zhang, Xuan Yang, Yandong Li, Tommi Jaakkola, Xuhui Jia, and Saining Xie. Inference-time scaling for diffusion models beyond scaling denoising steps, 2025.
- [28] Maxime Oquab, Timothée Darcet, Théo Moutakanni, Huy V. Vo, Marc Szafraniec, Vasil Khalidov, Pierre Fernandez, Daniel Haziza, Francisco Massa, Alaaeldin El-Nouby, Mido Assran, Nicolas Ballas, Wojciech Galuba, Russell Howes, Po-Yao Huang, Shang-Wen Li, Ishan Misra, Michael Rabbat, Vasu Sharma, Gabriel Synnaeve, Hu Xu, Hervé Jégou, Julien Mairal, Patrick Labatut, Armand Joulin, and Piotr Bojanowski. Dinov2: Learning robust visual features without supervision. *Trans. Mach. Learn. Res.*, 2024, 2024.
- [29] Byeongjun Park, Sangmin Woo, Hyojun Go, Jin-Young Kim, and Changick Kim. Denoising task routing for diffusion models, 2024.
- [30] William Peebles and Saining Xie. Scalable diffusion models with transformers. In *IEEE/CVF International Conference on Computer Vision, ICCV 2023, Paris, France, October 1-6, 2023*, pages 4172–4182. IEEE, 2023.
- [31] Alec Radford, Jong Wook Kim, Chris Hallacy, Aditya Ramesh, Gabriel Goh, Sandhini Agarwal, Girish Sastry, Amanda Askell, Pamela Mishkin, Jack Clark, Gretchen Krueger, and Ilya Sutskever. Learning transferable visual models from natural language supervision. In Marina Meila and Tong Zhang, editors, *Proceedings of the 38th International Conference on Machine Learning, ICML 2021, 18-24 July 2021, Virtual Event*, volume 139 of *Proceedings of Machine Learning Research*, pages 8748–8763. PMLR, 2021.
- [32] Robin Rombach, Andreas Blattmann, Dominik Lorenz, Patrick Esser, and Björn Ommer. High-resolution image synthesis with latent diffusion models. In *IEEE/CVF Conference on Computer Vision and Pattern Recognition, CVPR 2022, New Orleans, LA, USA, June 18-24, 2022*, pages 10674–10685. IEEE, 2022.
- [33] Olaf Ronneberger, Philipp Fischer, and Thomas Brox. U-net: Convolutional networks for biomedical image segmentation. In Nassir Navab, Joachim Hornegger, William M. Wells III, and Alejandro F. Frangi, editors, *Medical Image Computing and Computer-Assisted Intervention - MICCAI 2015 - 18th International Conference Munich, Germany, October 5 - 9, 2015, Proceedings, Part III*, volume 9351 of *Lecture Notes in Computer Science*, pages 234–241. Springer, 2015.
- [34] Chenyang Si, Ziqi Huang, Yuming Jiang, and Ziwei Liu. Freeu: Free lunch in diffusion u-net. *CoRR*, abs/2309.11497, 2023.
- [35] Jiaming Song, Chenlin Meng, and Stefano Ermon. Denoising diffusion implicit models. *CoRR*, abs/2010.02502, 2020.
- [36] Yang Song, Jascha Sohl-Dickstein, Diederik P Kingma, Abhishek Kumar, Stefano Ermon, and Ben Poole. Score-based generative modeling through stochastic differential equations. In *International Conference on Learning Representations*, 2021.
- [37] Jianlin Su, Murtadha Ahmed, Yu Lu, Shengfeng Pan, Wen Bo, and Yunfeng Liu. Roformer: Enhanced transformer with rotary position embedding. *Neurocomputing*, 568:127063, 2024.

- [38] Yuchuan Tian, Jing Han, Chengcheng Wang, Yuchen Liang, Chao Xu, and Hanting Chen. Dic: Rethinking conv3x3 designs in diffusion models. *CoRR*, abs/2501.00603, 2025.
- [39] Yuchuan Tian, Zhijun Tu, Hanting Chen, Jie Hu, Chao Xu, and Yunhe Wang. U-dits: Downsample tokens in u-shaped diffusion transformers, 2024.
- [40] Jiahao Wang, Ning Kang, Lewei Yao, Mengzhao Chen, Chengyue Wu, Songyang Zhang, Shuchen Xue, Yong Liu, Taiqiang Wu, Xihui Liu, Kaipeng Zhang, Shifeng Zhang, Wenqi Shao, Zhenguo Li, and Ping Luo. Lit: Delving into a simplified linear diffusion transformer for image generation, 2025.
- [41] Christopher Williams, Fabian Falck, George Deligiannidis, Chris C. Holmes, Arnaud Doucet, and Saifuddin Syed. A unified framework for u-net design and analysis. In Alice Oh, Tristan Naumann, Amir Globerson, Kate Saenko, Moritz Hardt, and Sergey Levine, editors, *Advances in Neural Information Processing Systems 36: Annual Conference on Neural Information Processing Systems 2023, NeurIPS 2023, New Orleans, LA, USA, December 10 - 16, 2023*, 2023.
- [42] Enze Xie, Junsong Chen, Junyu Chen, Han Cai, Haotian Tang, Yujun Lin, Zhekai Zhang, Muyang Li, Ligeng Zhu, Yao Lu, and Song Han. Sana: Efficient high-resolution image synthesis with linear diffusion transformer, 2024.
- [43] Yixing Xu, Chao Li, Dong Li, Xiao Sheng, Fan Jiang, Lu Tian, and Ashish Sirasao. Fdvit: Improve the hierarchical architecture of vision transformer. In *Proceedings of the IEEE/CVF International Conference on Computer Vision (ICCV)*, pages 5950–5960, October 2023.
- [44] Jingfeng Yao and Xinggang Wang. Reconstruction vs. generation: Taming optimization dilemma in latent diffusion models. *CoRR*, abs/2501.01423, 2025.
- [45] Sihyun Yu, Sangkyung Kwak, Huiwon Jang, Jongheon Jeong, Jonathan Huang, Jinwoo Shin, and Saining Xie. Representation alignment for generation: Training diffusion transformers is easier than you think. *CoRR*, abs/2410.06940, 2024.
- [46] Wangbo Zhao, Yizeng Han, Jiasheng Tang, Kai Wang, Yibing Song, Gao Huang, Fan Wang, and Yang You. Dynamic diffusion transformer. *arXiv preprint arXiv:2410.03456*, 2024.
- [47] Hongkai Zheng, Weili Nie, Arash Vahdat, and Anima Anandkumar. Fast training of diffusion models with masked transformers. *Trans. Mach. Learn. Res.*, 2024, 2024.
- [48] Zangwei Zheng, Xiangyu Peng, Tianji Yang, Chenhui Shen, Shenggui Li, Hongxin Liu, Yukun Zhou, Tianyi Li, and Yang You. Open-sora: Democratizing efficient video production for all, March 2024.

A Additional Experiments

In the appendix, we address the effect of proposed "Other Improvements" (Sec. 4), including "Time-aware MLP" and "Weight schedule of loss". These improvements bring slight increases on the generation metrics. Hence, we do not include them in the main experiments for the simplicity of the method.

ImageNet 256×256, w/ cfg		
Alignment Choices	FID↓	IS↑
Ordinary MLP	5.72	161.6
Time-aware MLP	5.63	163.3

Table 9: **The effect of time-aware MLPs.**

ImageNet 256×256, w/ cfg		
Alignment Choices	FID↓	IS↑
Constant	5.72	161.6
$\max(1, t + 0.5)$	5.85	161.3
$\max(1, -t + 1.5)$	5.72	161.6
$\min(1, \max(-2t + 1.5, 2t - 0.5))$	5.58	164.0

Table 10: **The effect of different weight schedules of loss.**